N73-23841

STUDY OF HYPERVELOCITY METEOROID IMPACT ON ORBITAL SPACE STATIONS

FINAL REPORT

April 1973

Contract NAS8-28473

CASE FILE COPY

Lockheed

HUNTSVILLE RESEARCH & ENGINEERING CENTER

LOCKHEED MISSILES & SPACE COMPANY, INC.
A SUBSIDIARY OF LOCKHEED AIRCRAFT CORPORATION

HUNTSVILLE, ALABAMA

HREC-8473-1
LMSC-HREC TR D306582

LOCKHEED MISSILES & SPACE COMPANY, INC.
HUNTSVILLE RESEARCH & ENGINEERING CENTER
HUNTSVILLE RESEARCH PARK
4800 BRADFORD DRIVE, HUNTSVILLE, ALABAMA

STUDY OF HYPERVELOCITY METEOROID IMPACT ON ORBITAL SPACE STATIONS

FINAL REPORT

April 1973

Contract NAS8-28473

Prepared for National Aeronautics and Space Administration
Marshall Space Flight Center, Alabama 35812

by

K. R. Leimbach

R. J. Prozan

APPROVED: John W. Benefield
John W. Benefield, Supervisor
Fluid Mechanics Section

J. S. Farrior
J. S. Farrior
Resident Director

FOREWORD

This document represents the final report of a study performed by Lockheed Missiles & Space Company, Inc., Huntsville Research & Engineering Center, entitled "Hypervelocity Meteoroid Impact on Orbital Space Stations," Contract NAS8-28473. The program was administered by the National Aeronautics and Space Administration's George C. Marshall Space Flight Center under the direction of Mr. David W. Jex, Space Sciences Laboratory.

The authors are grateful for the guidance and assistance provided by Mr. Jex in addition to Dr. L. Raman, Mr. R. L. Holland and Mr. G. Heintze.

SUMMARY

In the event of a hypervelocity impact of a meteorite on a spacecraft, structural damage may result. Of particular interest is the backside spallation caused by such a collision. To treat this phenomenon two numerical schemes were developed in the course of this study to compute the elastic-plastic flow and fracture of a solid. The numerical schemes are a five-point finite difference scheme and a four-node finite element scheme. The four-node finite element scheme proved to be less sensitive to the type of boundary conditions and loadings. Although further development work is needed to improve the program versatility (generalization of the network topology, secondary storage for large systems, improving of the coding to reduce the run time, etc.), the basic framework is provided for a utilitarian computer program which may be used in a wide variety of situations. Analytic results showing the program output are given for several test cases.

CONTENTS

Section		Page
	FOREWORD	ii
	SUMMARY	iii
	NOMENCLATURE	v
1	INTRODUCTION	1-1
2	EQUATIONS OF MOTION GOVERNING CONTINUOUS MEDIA	2-1
3	NUMERICAL ANALOGS TO THE GOVERNING EQUATIONS	3-1
	3.1 Five-Node Finite Difference Scheme	3-1
	3.2 Four-Node Finite Element Scheme	3-2
4	NUMERICAL RESULTS	4-1
5	CONCLUSIONS AND RECOMMENDATIONS	5-1
6	REFERENCES	6-1
Appendix		
A	USERS' MANUAL FOR THE COMPUTER PROGRAMS	A-1

NOMENCLATURE

Symbol	Description
A	surface area
a_1, a_2, a_3, b_1, b_2	coefficients of equation of state
C_o^2	damping coefficient for quadratic damping
C_s	scalar damping coefficient
E	energy of the control volume
e	internal energy per unit mass
f	any function
$\overline{F}_B, \overline{F}_B$	body force, body force per unit mass
$\overline{F}_s$	surface force
F_x, F_r	nodal forces
m	mass
p	pressure
$\overline{Q}$	heat transfer rate per unit area per unit time
$\mathfrak{Q}$	heat transferred into control volume
$\overline{\overline{q}}$	viscous deviator stress tensor
q'	viscous pressure
$\overline{S}$	position vector
t	time
u, v	displacements
V	volume

NOMENCLATURE (Continued)

Symbol	Description
W	work done on control volume
x, r, θ	cylindrical coordinate system coordinates
Y_o	yield modulus
Greek	
$\bar{\bar{\delta}}$	unit dyad (tensor)
$\delta_r, \delta_x, \delta_{rx}$	coordinate system rotation corrections
ϵ	strain
η	density/rest density ratio
λ	plastic flow correction factor
μ	shear modulus
μ_1	viscosity coefficient
ν	0 is planar motion, 1 is axisymmetric
ρ	density
$\bar{\bar{\sigma}}$	distortional stress deviator tensor
$\sigma_1, \sigma_2, \sigma_3$	principal stress
$\bar{\bar{\bar{\Sigma}}}$	stress tensor
ω	rotation angle
Superscripts	
$\cdot$	denotes time differentiation
e	designates element
n	denotes time step
Subscripts	
x, r, θ	denotes component in coordinate direction
xr	off diagonal term in stress and strain tensors
o	denotes rest condition

Section 1
INTRODUCTION

The analysis of dynamic response of elastic media to rapid loading, in particular meteorite impact, has been of considerable interest to the scientific community. Some of the most notable analytical investigations are given by MacCormack (Ref. 1), Rosenblatt (Ref. 2); Read and Bjork (Ref. 3) and Wilkins (Ref. 4). In these studies the emphasis has been placed on the dynamic response of the target or impacted material and on the response of the projectile.

Experimental studies (Ref. 5) have shown that for a given weight, a thin meteorite bumper arrangement gives better protection than a single skin. The purpose of the bumper is not necessarily to completely stop the incoming projectile but to at least absorb some of the incident energy before failing under the applied load. Backside spallation of the bumper then scatters fragments of both the meteorite and the bumper material which in turn strike the structural skin. These fragments possess a lower total energy and also impact the structural surface over a much wider area thus decreasing the peak loading.

Development of the bumper approach created a need for an analysis which treats the fracture phenomena of a material. It is the purpose of this study to provide this capability. The schemes chosen are based on combinations of ideas found in the above references and the work of Ang (Refs. 6, 7, 8). Of the two schemes investigated, a five-node finite difference scheme and a finite element scheme, the finite element scheme produced the best numerical behavior. It can be shown that the finite element treatment actually is analogous to a nine-point finite difference scheme. The additional four points enhance the stability characteristics (with respect to the five-point scheme).

In the following discussion both approaches are discussed. Computer programs have been written to conduct the calculation and are briefly discussed in this report.

Section 2
EQUATIONS OF MOTION GOVERNING CONTINUOUS MEDIA

For a control mass in motion conservation of mass becomes

$$\frac{dm}{dt} = \frac{d}{dt}\int_{cv} \rho dV = 0 \quad . \tag{2.1}$$

from Newton's second law we get

$$\frac{d}{dt}\left(m\dot{\bar{S}}_{mc}\right) = \int_{cs} d\bar{F}_s + \int_{cv} d\bar{F}_B \tag{2.2}$$

while the first law of thermodynamics yields

$$\frac{dE}{dt} = \frac{d\mathfrak{Q}}{dt} + \frac{dW}{dt} \quad . \tag{2.3}$$

Now the velocity of the mass center is

$$\dot{\bar{S}}_{mc} = \int_{cv} \rho\dot{\bar{S}}\, dV/m$$

so that Eq. (2.3) becomes

$$\frac{d}{dt}\int_{cv} \rho\dot{\bar{S}}\, dV = \int_{cs} d\bar{F}_s + \int_{cv} d\bar{F}_B$$

The work done on the control volume in time dt is

$$\Delta W = \int_{cs} d\bar{F}_s \cdot d\bar{S} + \int_{cv} \rho\bar{f}_B \cdot d\bar{S}\, dV$$

where $d\overline{S}$ is the distance moved in that time so that the instantaneous rate of work done on the control volume is

$$\dot{W} = \int_{cs} \dot{\overline{S}} \cdot d\overline{F}_s + \int_{cv} \rho \dot{\overline{S}} \cdot \overline{f}_B \, dV$$

The rate of change of energy contained within the control volume is

$$\dot{E} = \int_{cv} \rho \left\{ e + \tfrac{1}{2} \dot{\overline{S}} \cdot \dot{\overline{S}} \right\} dV$$

It is convenient to express $\frac{d\mathcal{Q}}{dt}$ as $\int_{cs} \overline{Q} \cdot d\overline{A}$ where $\overline{Q}$ is the heat transfer vector per unit time per unit area. In a similar fashion let

$$d\overline{F}_s = \overline{\overline{\Sigma}} \cdot d\overline{A}$$

so that the governing equations can be summarized as below

$$\frac{d}{dt} \int_{cv} \rho dV = 0 \tag{2.4a}$$

$$\frac{d}{dt} \int_{cv} \rho \dot{\overline{S}} \, dV = \int_{cs} \overline{\overline{\Sigma}} \cdot d\overline{A} + \int_{cv} \rho \overline{f}_B \, dV \tag{2.4b}$$

$$\frac{d}{dt} \int_{cv} \rho \left(e + \tfrac{1}{2} \dot{\overline{S}} \cdot \dot{\overline{S}}\right) dV = \int_{cs} \left(\overline{Q} + \dot{\overline{S}} \cdot \overline{\overline{\Sigma}}\right) \cdot d\overline{A} + \int_{cv} \rho \dot{\overline{S}} \cdot \overline{f}_B \, dV \tag{2.4c}$$

where the control surface is determined by the space time history of points on the original or starting surface.

Assuming continuous functions within the region we may write, with the aid of Gauss' theorem, for momentum and energy

$$\rho \ddot{\bar{S}} = \nabla \cdot \bar{\bar{\Sigma}} + \rho \bar{f}_B \tag{2.5a}$$

$$\rho \left(\dot{e} + \dot{\bar{S}} \cdot \ddot{\bar{S}}\right) = \nabla \cdot \left(\bar{Q} + \dot{\bar{S}} \cdot \bar{\bar{\Sigma}}\right) + \rho \dot{\bar{S}} \cdot \bar{f}_B \tag{2.5b}$$

Combining (2.5a) and (2.5b) yields

$$\rho \dot{e} = \nabla \cdot \bar{Q} + \left(\bar{\bar{\Sigma}} \cdot \nabla\right) \cdot \dot{\bar{S}} \tag{2.6}$$

At this point it is convenient to decompose the dyad (or second order tensor) $\bar{\bar{\Sigma}}$ into viscous and inviscid components viz:

$$\bar{\bar{\Sigma}} = \bar{\bar{\Sigma}}_I + \bar{\bar{\Sigma}}_v = \bar{\bar{\sigma}} - p\bar{\bar{\delta}} - q'\bar{\bar{\delta}} - \bar{\bar{q}}$$

Now $\bar{\bar{\sigma}}$ is the deviator stress tensor due to elastic/plastic distortions, p is the hydrostatic pressure, q' the viscous pressure and $\bar{\bar{q}}$ is the deviator viscous stress tensor. The elastic stress convention is such that tension yields a positive stress while pressure in hydrodynamics is usually defined in the opposite sense. The viscous stresses usually are defined in the same sense as pressure.

Assuming an axially symmetric motion (or a planar one) the equations of motion may be written,

$$\rho \ddot{r} = \frac{\partial \Sigma_r}{\partial r} + \frac{\partial \Sigma_{rx}}{\partial x} + \nu \left(\frac{\Sigma_r - \Sigma_\theta}{r}\right) \tag{2.7a}$$

$$\rho \ddot{x} = \frac{\partial \Sigma_{rx}}{\partial r} + \frac{\partial \Sigma_x}{\partial x} + \nu \left(\frac{\Sigma_{rx}}{r}\right) \tag{2.7b}$$

for a cylindrical coordinate system.

The equation of continuity becomes

$$\frac{\dot{V}}{V} = \dot{\epsilon}_r + \dot{\epsilon}_x + \nu\dot{\epsilon}_\theta \tag{2.7c}$$

where the strain rates are;

$$\begin{aligned}
\dot{\epsilon}_r &= \frac{\partial \dot{r}}{\partial r} = \frac{\partial \dot{v}}{\partial r} \\
\dot{\epsilon}_x &= \frac{\partial \dot{x}}{\partial x} = \frac{\partial \dot{u}}{\partial x} \\
\dot{\epsilon}_\theta &= \frac{\dot{r}}{r} = \frac{\dot{v}}{r} \\
\dot{\epsilon}_{rx} &= \frac{\partial \dot{r}}{\partial x} + \frac{\partial \dot{x}}{\partial r} = \frac{\partial \dot{v}}{\partial x} + \frac{\partial \dot{u}}{\partial r}
\end{aligned} \tag{2.8}$$

The material law for linear elastic isotropic homogeneous material is

$$\begin{aligned}
\dot{\sigma}_r &= 2\mu\left(\dot{\epsilon}_r - \frac{1}{3}\frac{\dot{V}}{V}\right) + \dot{\delta}_r \\
\dot{\sigma}_x &= 2\mu\left(\dot{\epsilon}_x - \frac{1}{3}\frac{\dot{V}}{V}\right) + \dot{\delta}_x \\
\dot{\sigma}_\theta &= 2\mu\left(\dot{\epsilon}_\theta - \frac{1}{3}\frac{\dot{V}}{V}\right) \text{ (axisymmetric only)} \\
\dot{\sigma}_{rx} &= \mu\dot{\epsilon}_{rx} + \dot{\delta}_{rx}
\end{aligned} \tag{2.9}$$

The quantities δ_r, δ_x, δ_{rx} are corrections to account for the rotation of the coordinate system.

Consider the rotation of the coordinate system by an angle ω. Then

$$\begin{aligned}
\delta_r &= (\Sigma_x - \Sigma_r)\sin^2\omega - 2\Sigma_{rx}\sin\omega\cos\omega \\
\delta_x &= -\delta_r \\
\delta_{rx} &= -2\Sigma_{rx}\sin^2\omega - (\Sigma_x - \Sigma_r)\sin\omega\cos\omega
\end{aligned} \tag{2.10}$$

but

$$\dot{\omega} = \nabla \times (u\bar{i} + v\bar{j})$$

Equations (2.9) could be differentiated with respect to time but there is no need since the integral is the quantity that is really required.

Expansion of Eq. (2.6) yields

$$\rho\dot{e} = \Sigma_x \dot{\epsilon}_x + \Sigma_r \dot{\epsilon}_r + \Sigma_\theta \dot{\epsilon}_\theta + \Sigma_{xy} \dot{\epsilon}_{xy}$$

which yields

$$\rho\dot{e} = -(p+q')\frac{\dot{V}}{V} + (\sigma_x - q_x)\dot{\epsilon}_x + (\sigma_r - q_r)\dot{\epsilon}_r + (\sigma_\theta - q_\theta)\dot{\epsilon}_\theta \qquad (2.11)$$

$$+ (\sigma_{xr} - q_{xr})\dot{\epsilon}_{xr}$$

The hydrostatic pressure must be obtained from an equation of state. Functionally we may express this as

$$p = p(\rho, e)$$

The form used by Wilkins (Ref. 4) is

$$p = a_1(\eta - 1) + a_2(\eta - 1)^2 + a_3(\eta - 1)^3 + \left[b_1(n-1) + b_2(\eta - 1)^2\right] e$$

where $\eta = \rho/\rho_o$ and is the functional used in this study.

To complete the governing equations the viscosity must be discussed. Generally speaking in numerical analysis the introduction of viscosity occurs more frequently to enhance stability of the numerical solution than for the purpose of treating internal damping or viscous effects. As such the viscosity models are created to control some undesirable behavior and do not

necessarily have firm underlying mathematical principles. Several mathematical models were tested in the subject analysis. These are: (1) Linear Damping; (2) Quadratic Damping; (3) Velocity Angular Distortion; (4) Spatial Angular Distortion; and (5) Spatial Displacement Distortion.

The first method has firm mathematical grounding in the sense that it is a conventional model for fluids obeying the Reiner-Revlin law. The second method uses a first coefficient of viscosity which is proportional to the divergence and a second coefficient which is zero. The last three methods are artificially contrived. The third was suggested by Wilkins (Ref. 4) to control an undesirable "hourglass" distortion. The last two were developed in this study due to the inadequacy of the five point lattice scheme to "remember" what the original rest configuration was and to return to that state in the absence of disturbing forces.

In the scalar damping

$$q' = C_s \mu_1 \frac{\dot{V}}{V} \tag{2.12a}$$

$$q_r = 2\mu_1 (\dot{\epsilon}_r - \frac{1}{3} \frac{\dot{V}}{V}) \tag{2.12b}$$

$$q_x = 2\mu_1 (\dot{\epsilon}_x - \frac{1}{3} \frac{\dot{V}}{V}) \tag{2.12c}$$

$$q_\theta = 2\mu_1 (\dot{\epsilon}_\theta - \frac{1}{3} \frac{\dot{V}}{V}) \tag{2.12d}$$

$$q_{rx} = \mu_1 \dot{\epsilon}_{rx} \tag{2.12e}$$

while in the quadratic damping

$$q' = C_o^2 \rho_o (\frac{\dot{V}}{V})^2 \tag{2.13}$$

A departure from Wilkins is taken in that the factor $\frac{A}{V}$ was omitted in the quadratic damping since it precluded a uniform radial distribution in cases where no variations of properties in the radial direction can be expected.

The remaining topics of yield and fracture complete the governing equations discussion. The principal stresses are

$$\sigma_{1,2} = \frac{\sigma_r + \sigma_x}{2} \pm \frac{1}{2} \sqrt{(\sigma_r + \sigma_x)^2 + (2\sigma_{rx})^2} \tag{2.14}$$

and

$$\sigma_3 = \sigma_\theta \quad \text{(axisymmetric only)}$$

The yield condition is given by Von Mises as

$$\sigma_1^2 + \sigma_2^2 + \sigma_3^2 - \frac{2}{3} (Y_o)^2 \leq 0$$

If this condition is not satisfied then all stresses are corrected by multiplying by the factor

$$\lambda = \frac{\sqrt{\frac{2}{3}}\, Y_o}{\sqrt{\sigma_1^2 + \sigma_2^2 + \sigma_3^2}}$$

The validity of this procedure is discussed by Hill (Ref. 9). A fracture occurs if the principal tensile stress exceeds the ultimate tensile strength.

This concludes the discussion of the governing equations for the continuous media. The numerical analogs are developed in the following section.

Section 3
NUMERICAL ANALOGS TO THE GOVERNING EQUATIONS

3.1 FIVE-NODE FINITE DIFFERENCE SCHEME

This is the simplest numerical analog possible, at least with regard to the region of influence. For each node point in the array the positions, displacements, stresses, pressure, viscosity, and velocities are stored. Figure 1 illustrates a typical interior node.

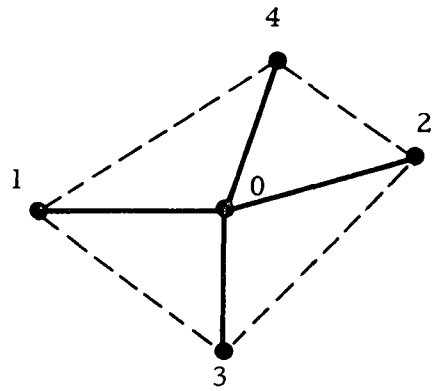

Fig. 1 - Typical Five-Node Lattice Numbering Scheme

The spatial derivatives of any function f are

$$\frac{\partial f}{\partial x} = \frac{1}{2A} \left\{ (f_2 - f_1)(r_4 - r_3) - (f_4 - f_3)(r_2 - r_1) \right\} \tag{3.1.1}$$

$$\frac{\partial f}{\partial r} = -\frac{1}{2A} \left\{ (f_2 - f_1)(x_4 - x_3) - (f_4 - f_3)(x_2 - x_1) \right\} \tag{3.1.2}$$

The accelerations are computed using Eqs. (2.7a) and (2.7b). Integration of the accelerations yields new velocities over the entire field while a second integration yields the new positions and displacements. Using the above

information the strain rates at the new time may be found from Eqs. (2.8) while the new deviator stress distributions are found by integrating Eqs. (2.9).

The pressure and energy may then be evaluated and the new viscous terms determined. From this information the updated stress tensor is found.

A special matrix is retained which for each node point stores the index of the point to the left, right, top and bottom. In the event that point 0 is on the left boundary the index for point 1 is set to that of point 0 and a one sided derivative results. This process is used for all peripheral points. As will be seen later the unconstrained corner point such as shown (Fig. 2) has poor stability and constitutes the greatest problem with the five-point method.

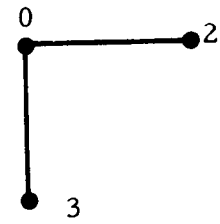

Fig. 2 - Degeneration of Five-Point Grid at Corner Point

Boundary conditions are treated with special subroutines which reset displacements, velocities and stresses in an appropriate fashion. These routines are extremely flexible such that any type of boundary conditions may be treated by recoding rather than by data card input. Very few cards are involved, typically 5 to 10, in this recoding. This approach was considered superior to a complex input setup in which every conceivable type of boundary condition was anticipated.

3.2 FOUR-NODE FINITE ELEMENT SCHEME

This computer program features some of the aspects of the traditional finite element programs used in structural analysis. Dynamic core storage allocation is used for the major size-dependent variables, which are grouped

in nodal quantities (position coordinates, displacements, velocities, forces, masses) and regional quantities (stresses, pressure, scalar viscosity, total energy and distortional energy).

The elastic-plastic continuum is replaced by four-node regions (elements) as shown on Fig. 3. The corner points are numbered 1 through 4 counterclockwise. The state of stress in the element is assumed to be constant.

The mass characteristics of the continuum are modeled as discrete lumps located at the node points (Fig. 4). The motion of the continuum is treated in terms of the motion of these lumps.

The equation of motion is simply a sum of all forces, elastic and inertia, acting on the lump. No special logic is required for boundary lumps since the elastic forces are summed as the element stresses for each element are updated. This simplifies the coding considerably, doing away with special features for various types of boundaries. The equation of motion may be stated as

$$m\ddot{x} = \sum_e F_x^e \tag{3.2.1}$$

$$m\ddot{r} = \sum_e F_r^e \tag{3.2.2}$$

where F_x^e and F_r^e are the elastic (spring) forces of the elements holding lump m.

The velocities are obtained by taking

$$\dot{x}^{n+\frac{1}{2}} = \dot{x}^{n-\frac{1}{2}} + \frac{\sum_e F_x^e \, \Delta t^{n+1}}{m} \tag{3.2.3}$$

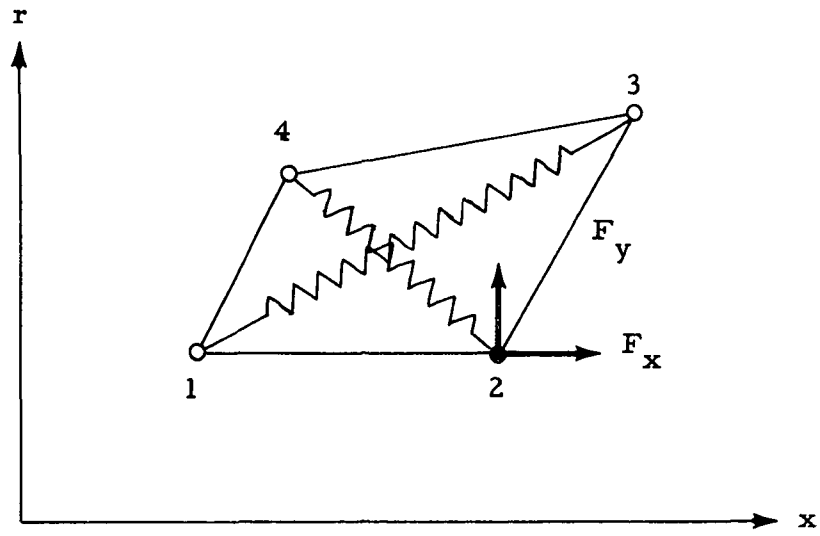

Fig. 3 - Four-Node Element

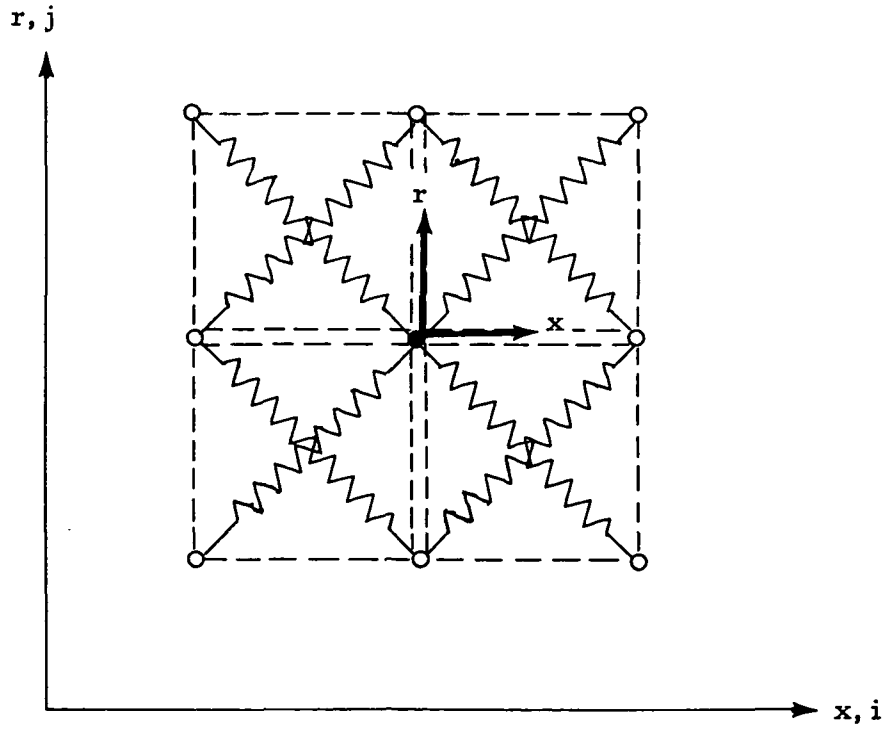

Fig. 4 - Typical Node With Surrounding Elements

$$\dot{r}^{n+\frac{1}{2}} = \dot{r}^{n-\frac{1}{2}} + \frac{\sum_e F_r^e \, \Delta t^{n+1}}{m} \tag{3.2.4}$$

If a velocity boundary condition is imposed the affected nodal velocities computed from Eqs. (3.2.5) and (3.2.6) are simply reset to the imposed values. Force boundary conditions, such as externally applied forces, are imposed before Eqs. (3.2.5) and (3.2.6) are executed.

In another integration step the displacements are computed,

$$u^{n+1} = u^n + \dot{x}^{n+\frac{1}{2}} \, \Delta t^{n+\frac{1}{2}} \tag{3.2.5}$$

$$v^{n+1} = v^n + \dot{r}^{n+\frac{1}{2}} \, \Delta t^{n+\frac{1}{2}} \tag{3.2.6}$$

Displacement boundary conditions may also be imposed.

Now the element quantities can be computed based on the new velocities and displacements, from the equations of motion.

A fracture condition has been added, which severs the springs representing the strength of the element. This fracture occurs when the principal tensile stress exceeds the ultimate tensile strength of the material.

The corner forces are computed for the element based on the new stresses and damping terms. The directional damping terms are not stored. These corner forces are

$$\begin{aligned}
F_{x1} &= -\tfrac{1}{2}\left[(\Sigma_{x1}(r_2 - r_4) - \Sigma_{xr}(x_2 - x_4)\right]\bar{r} + \tfrac{1}{4}\Sigma_{xr} A\Big|^* \\
F_{x2} &= -\tfrac{1}{2}\left[(\Sigma_{x2}(r_3 - r_1) - \Sigma_{xr}(x_3 - x_1)\right]\bar{r} + \tfrac{1}{4}\Sigma_{xr} A\Big|^* \\
F_{x3} &= -\tfrac{1}{2}\left[(\Sigma_{x3}(r_4 - r_2) - \Sigma_{xr}(x_4 - x_2)\right]\bar{r} + \tfrac{1}{4}\Sigma_{xr} A\Big|^* \\
F_{x4} &= -\tfrac{1}{2}\left[(\Sigma_{x4}(r_1 - r_3) - \Sigma_{xr}(x_1 - x_3)\right]\bar{r} + \tfrac{1}{4}\Sigma_{xr} A\Big|^*
\end{aligned} \tag{3.2.7}$$

$$
\begin{aligned}
F_{r1} &= \tfrac{1}{2}\left[\Sigma_{y1}(x_2 - x_4) - \Sigma_{xy}(r_2 - r_4)\right]\bar{r} + \frac{1}{4}(\Sigma_r - \Sigma_\theta)\ A\Big|^* \\
F_{r2} &= \tfrac{1}{2}\left[\Sigma_{y2}(x_3 - x_1) - \Sigma_{xy}(r_3 - r_1)\right]\bar{r} + \frac{1}{4}(\Sigma_r - \Sigma_\theta)\ A\Big|^* \\
F_{r3} &= \tfrac{1}{2}\left[\Sigma_{y3}(x_4 - x_2) - \Sigma_{xy}(r_4 - r_2)\right]\bar{r} + \frac{1}{4}(\Sigma_r - \Sigma_\theta)\ A\Big|^* \\
F_{r4} &= \tfrac{1}{2}\left[\Sigma_{y4}(x_1 - x_3) - \Sigma_{xy}(r_1 - r_3)\right]\bar{r} + \frac{1}{4}(\Sigma_r - \Sigma_\theta)\ A\Big|^*
\end{aligned}
\tag{3.2.10}
$$

$\bar{r} = 1$; $\Big|^* = 0$ for plane strain problems.

Section 4
NUMERICAL RESULTS

To investigate the numerical problems involved in the computation of elastic-plastic flow a one-dimensional code was written and implemented. A wave propagation problem given by Wilkins (Ref. 4) was checked with this code using two different mesh sizes (250 and 50 node points). The material is described by P=0, $\rho_o = 4 g/cm^3$ $\mu = 3$ Mb and $Y_o = \infty$. The left boundary of the 5 cm thick plate is excited by $\dot{x} = -10^{-3} \sin 2\pi t$ cm/μ sec.

The stress waves are depicted on Figs. 4-1 through 4-3.

The five-node finite difference scheme was first tested on a one-dimensional problem although the calculations were performed two-dimensionally. Quadratic damping was used in this test case. A uniform velocity was imposed at one end of a rod while the other end was fixed. The rod was constrained to slide in a tube such that no vertical displacement was possible. The axial velocities resulting from the improved boundary conditions are shown in Fig. 4-4 for several node points. As the time approached infinity the internal oscillations damped and a linear velocity distribution throughout the rod was achieved.

The two-dimensional codes initially suffered from stability problems. The examples shown were taken again from Wilkins, with the material data $P = 1.88\ (\eta - 1)$ Mb, $\rho_o = 7.72\ g/cm^3$, $\mu = 0.814$ Mb and $Y_o = \infty$. The cantilever plate is 1.00 by 5.25 cm, the fixed-fixed plate is 1.00 by 10.50 cm. The excitation was achieved by supplying a boundary velocity.

Figures 4-5 and 4-6 show how the upper edge of the cantilever plate is set into motion at constant velocity and constant rotation, respectively. Relatively smooth deformation patterns result. If an edge is released, however, instability occurs almost immediately (Fig. 4-7). This points to a weakness in the formation in the edge condition of the five-point scheme. For all three plots the deformations are magnified ten-fold.

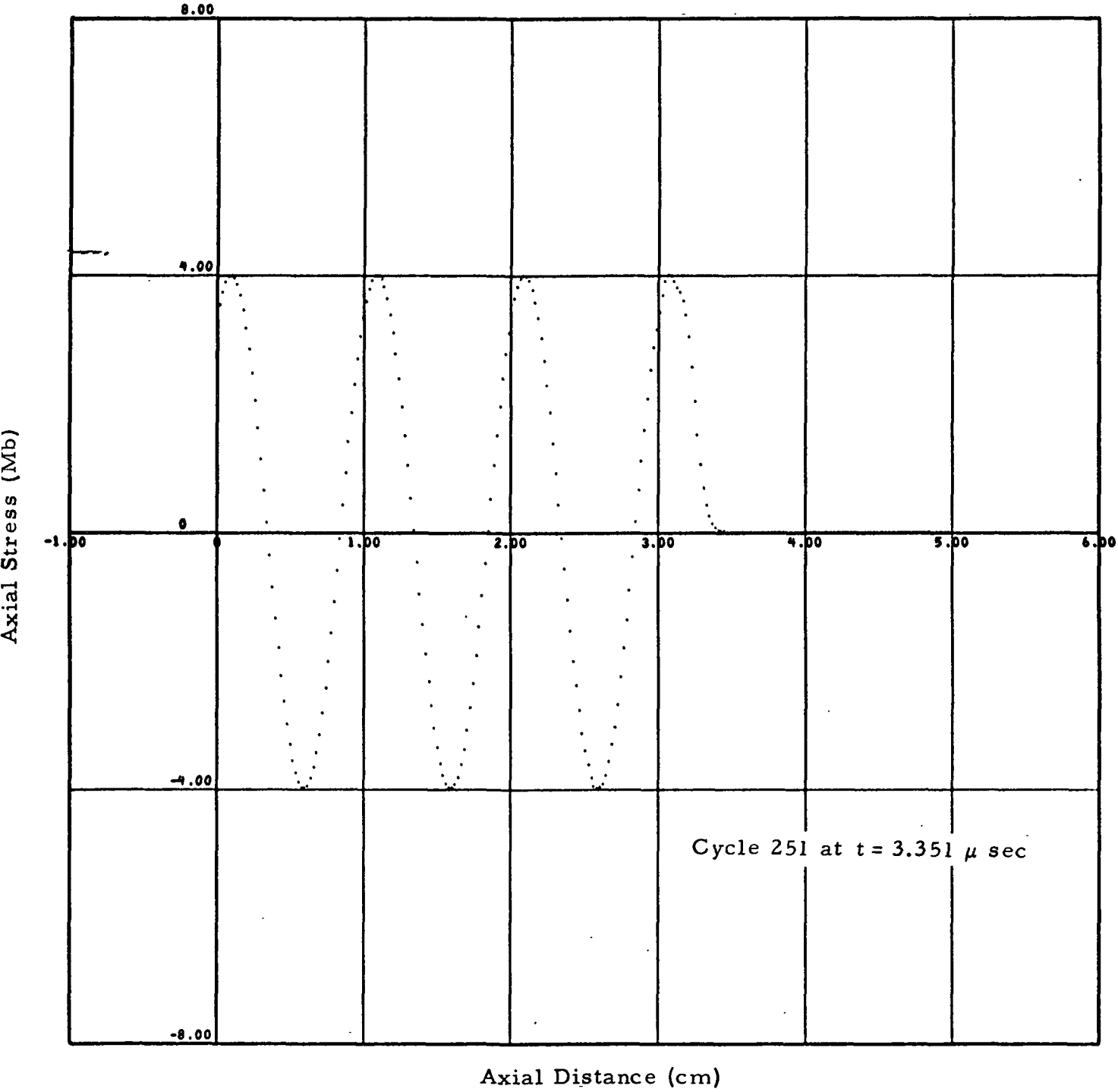

Fig. 4-1 - Stress Distribution in the Plate

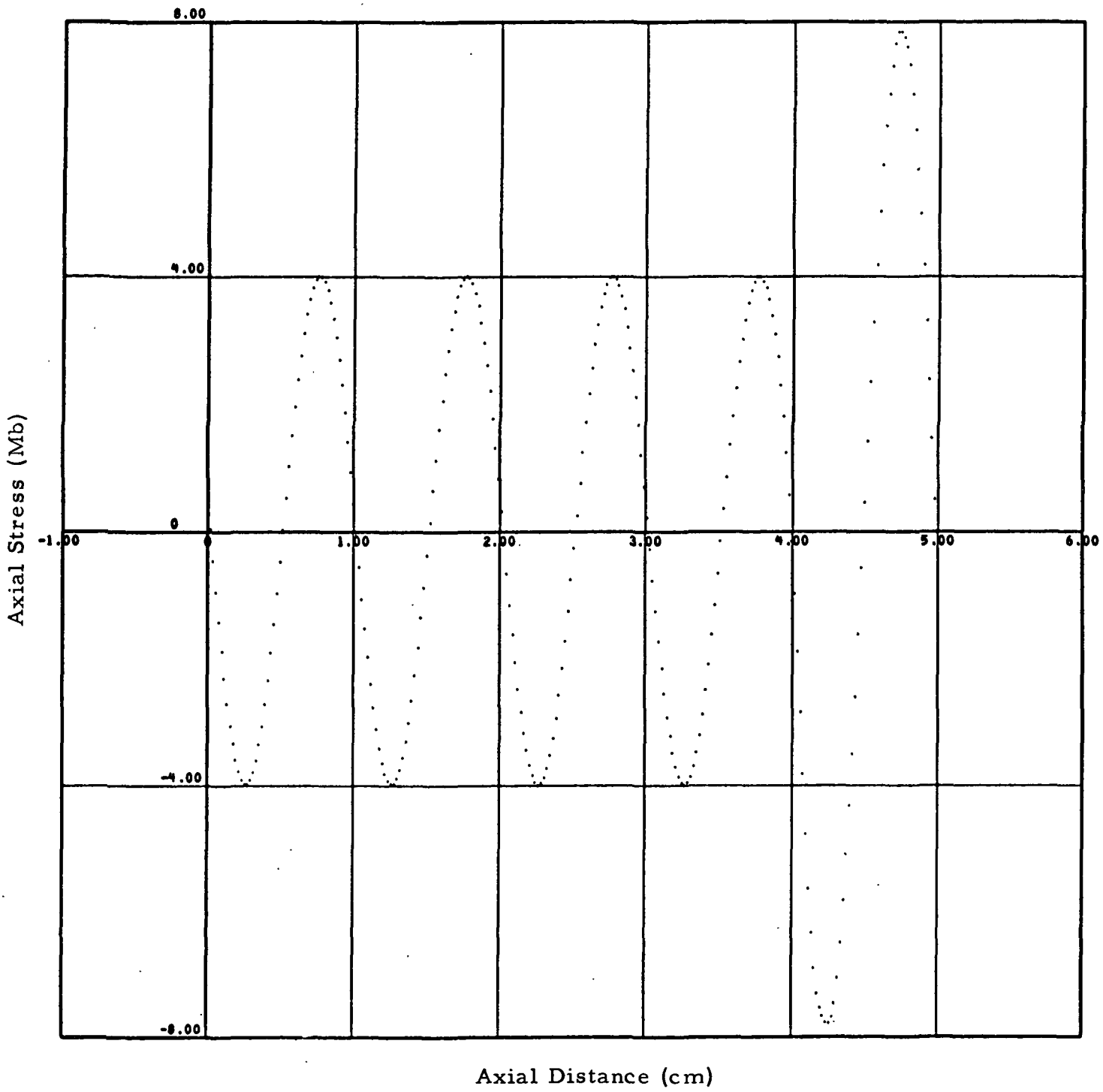

Fig. 4-2 - Reflection of the Wave at the Free Boundary

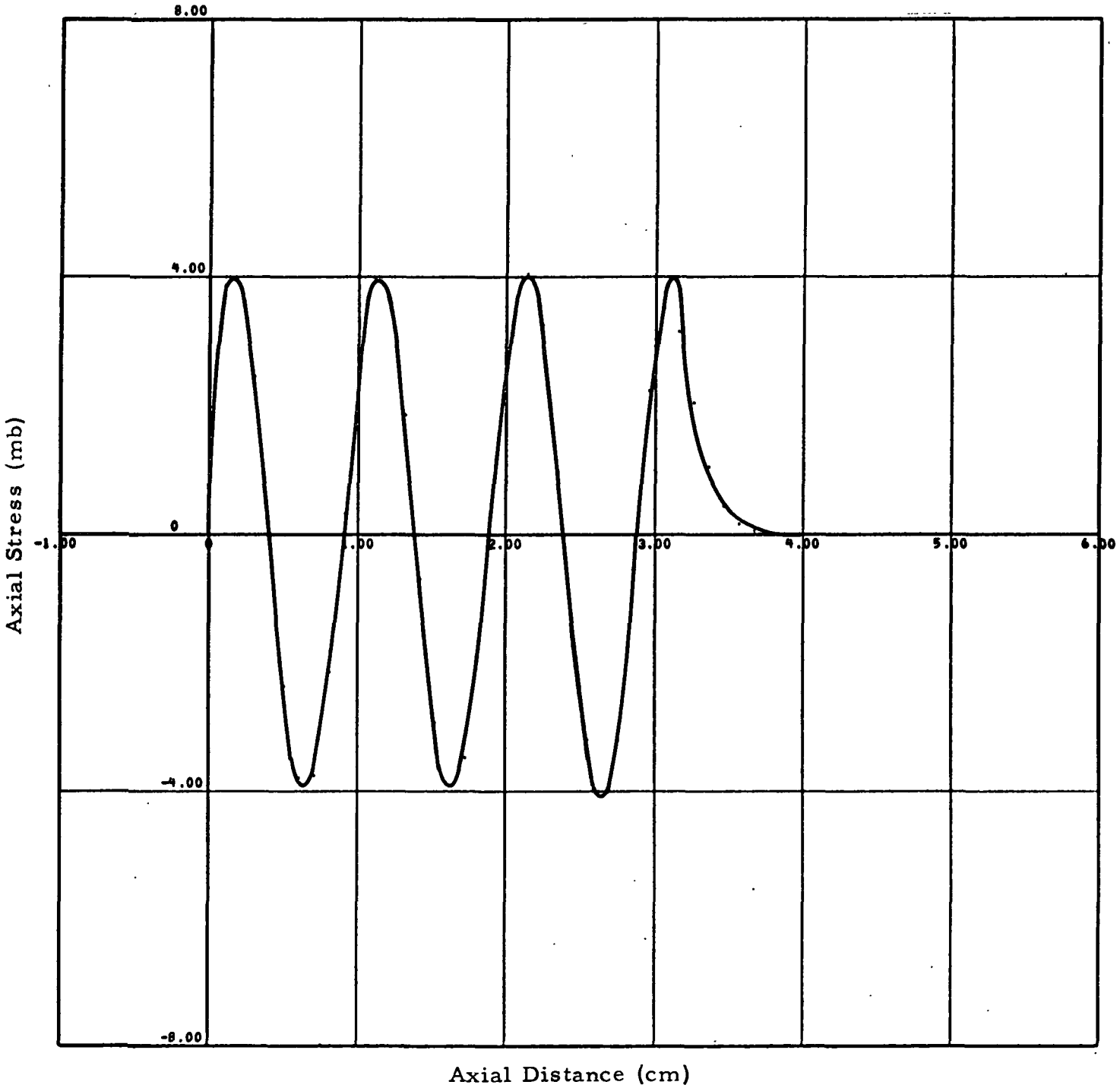

Fig. 4-3 - Stress Distribution for Coarse Mesh at t = 3.3 μ sec

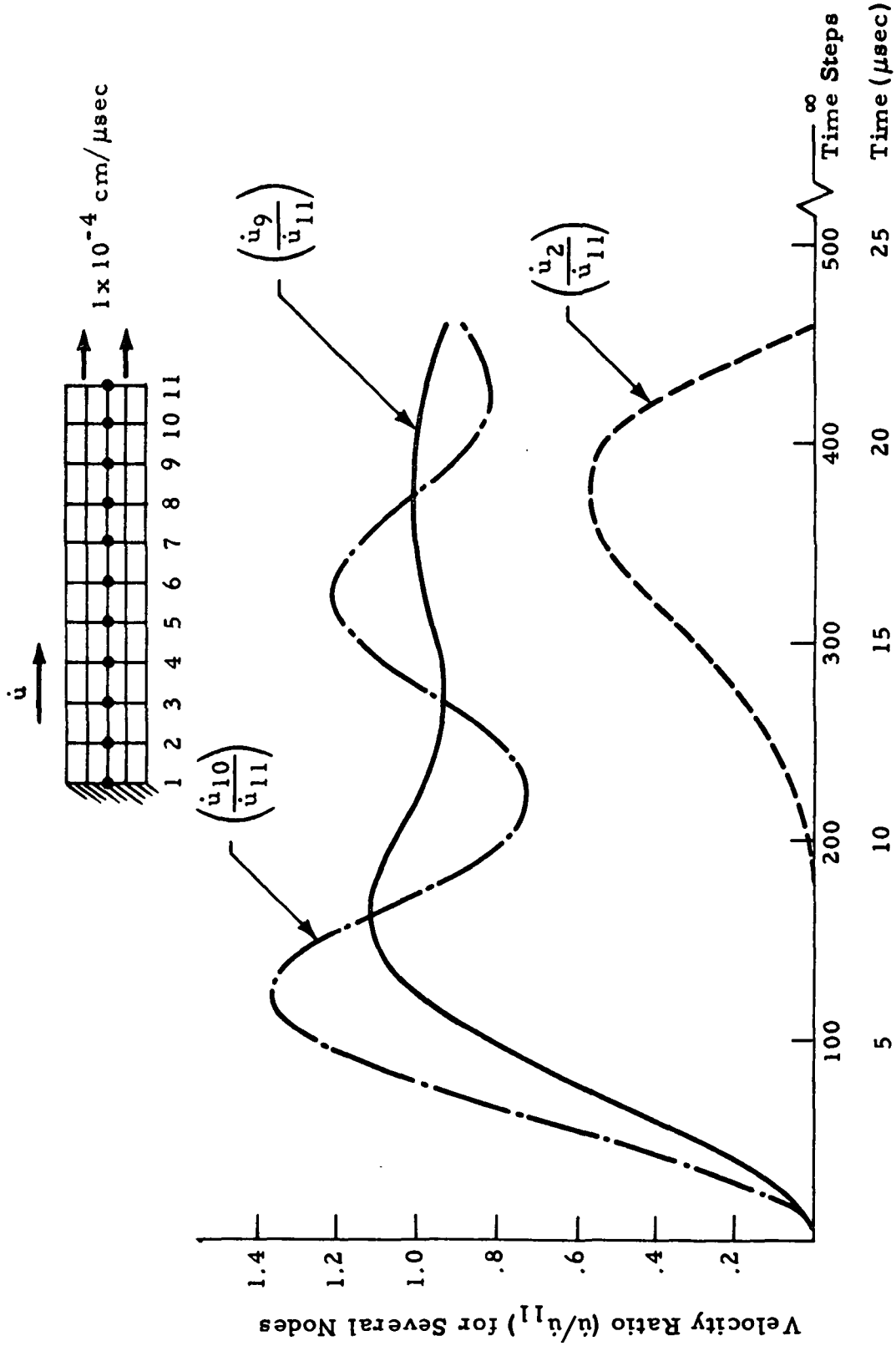

Fig. 4-4 - Theoretical Velocity vs Time History at Several Points on an Aluminum Bar

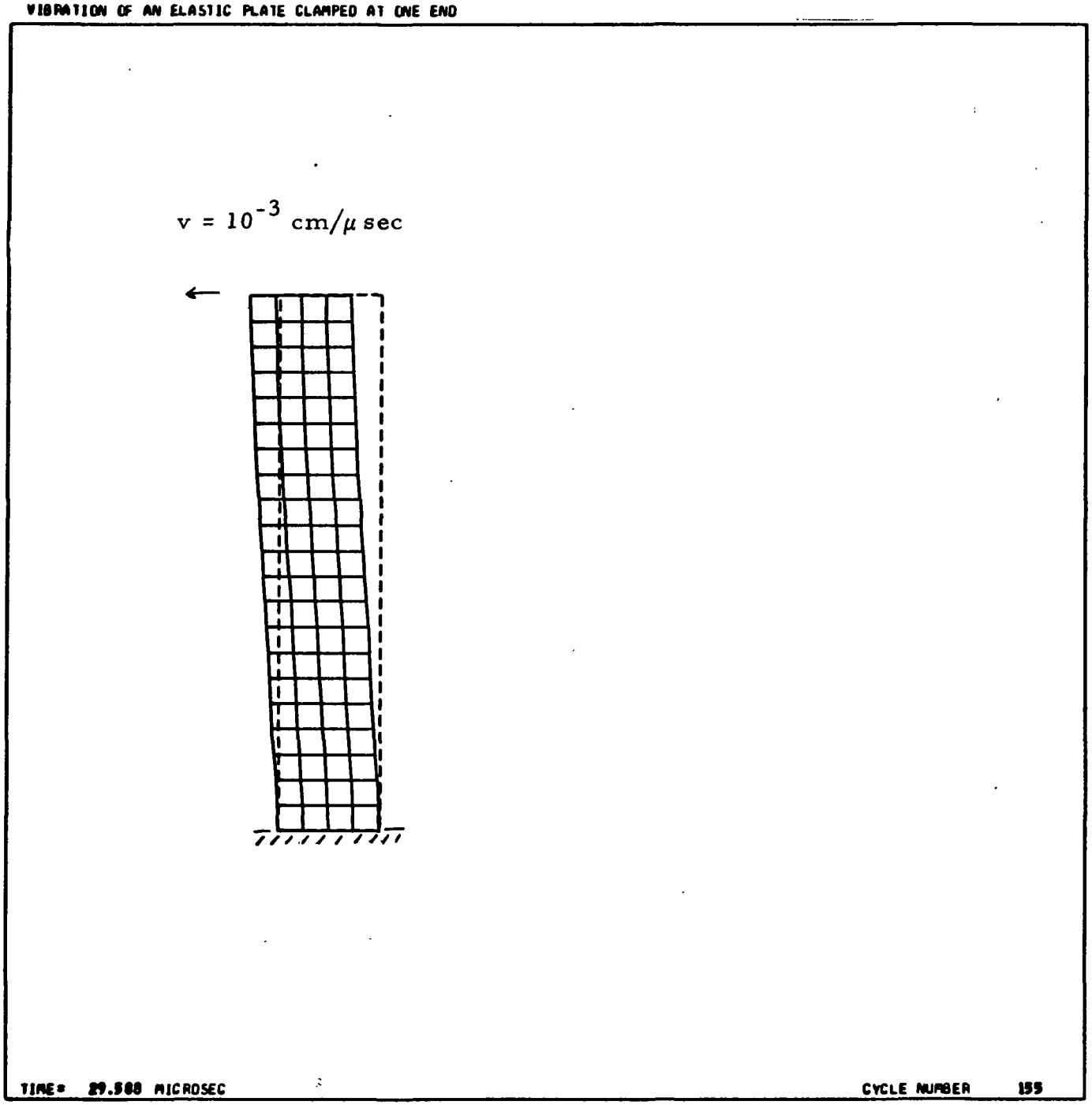

Fig. 4-5 - Elastic Shear Deformation (Five-Point Scheme, Plane Strain)

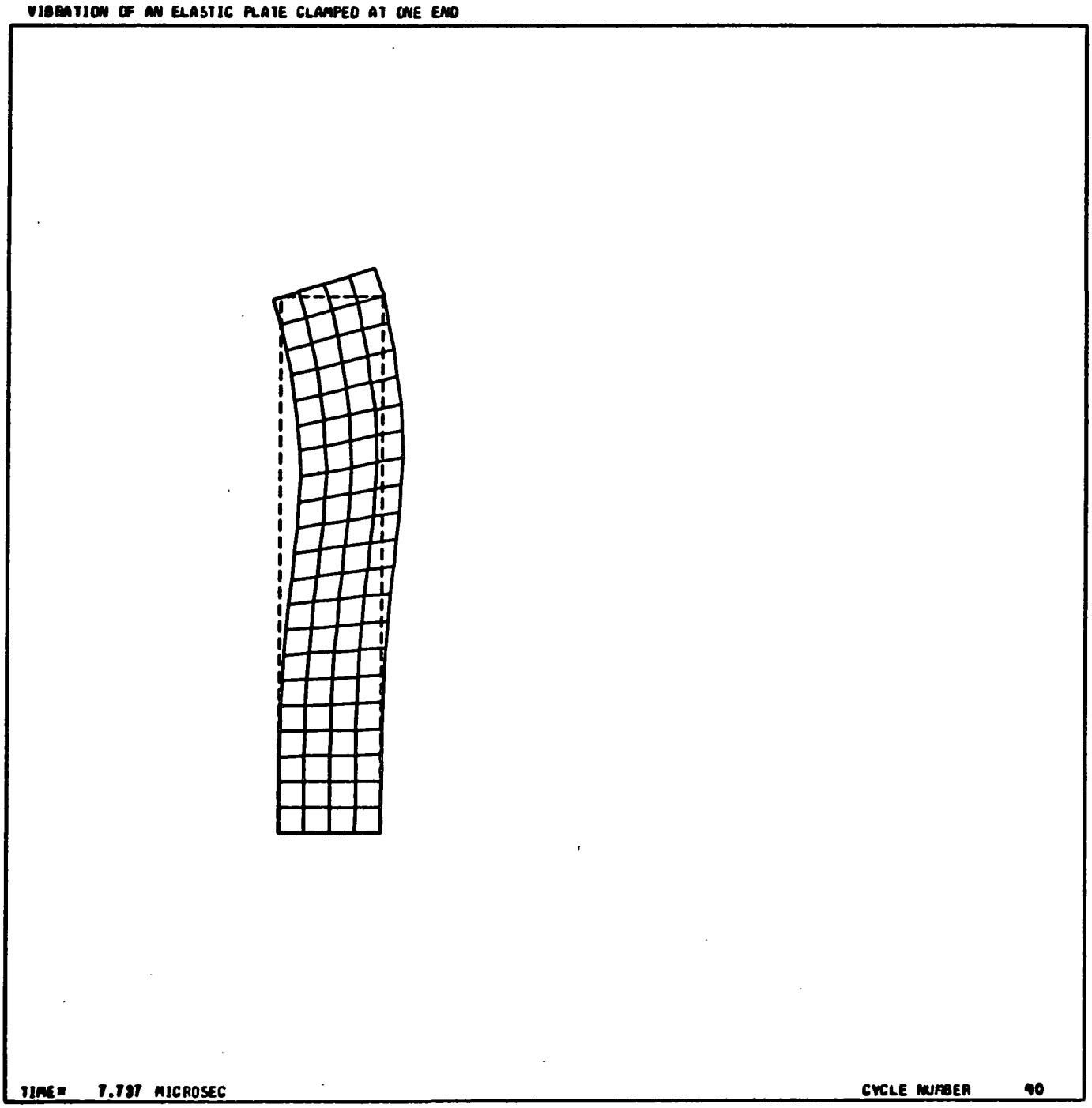

Fig. 4-6 - Elastic Bending Deformation (Five-Point Scheme, Plane Strain)

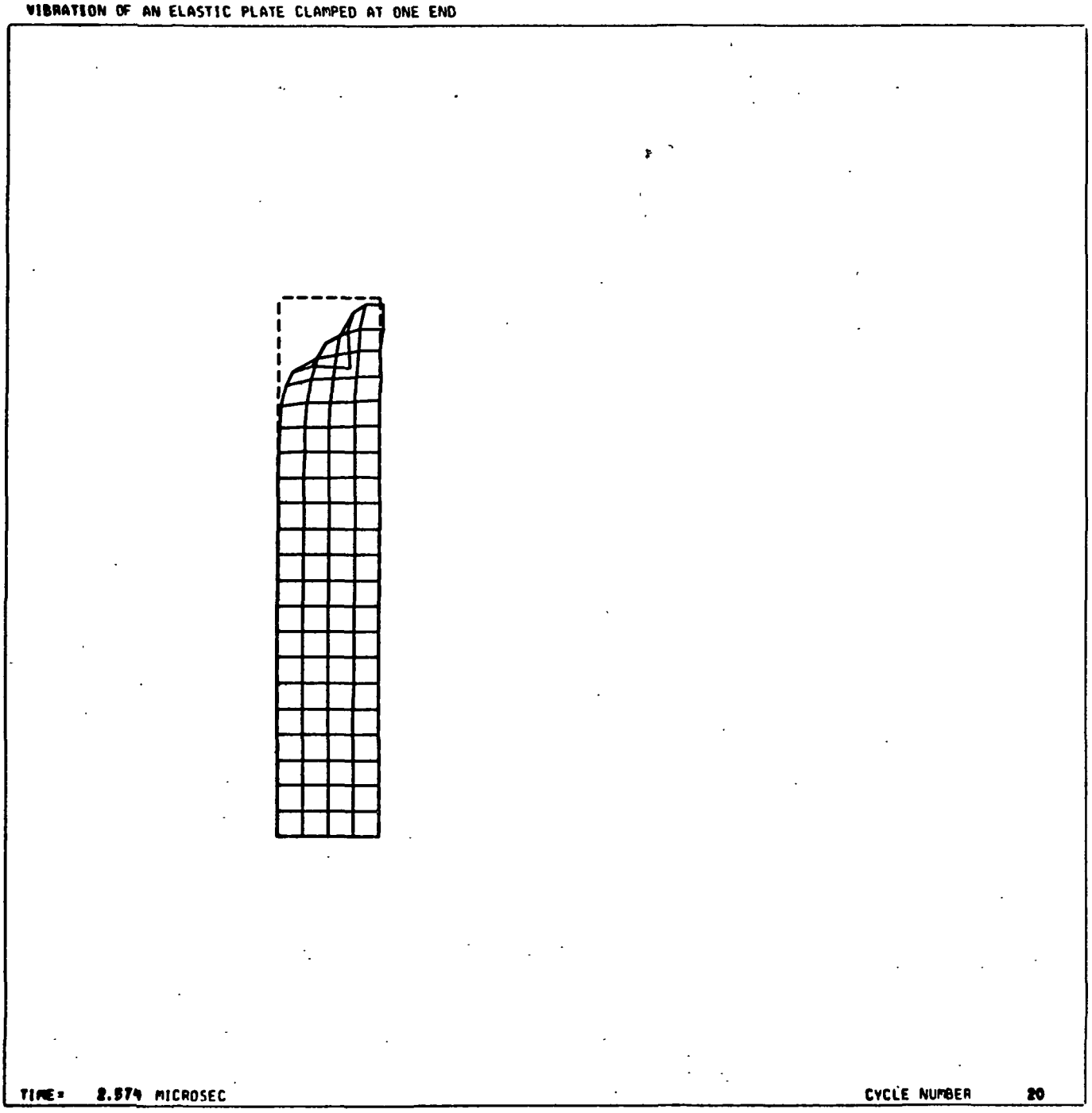

Fig. 4-7 - Instability of the Five-Point Scheme at the Corner Points

The fixed-fixed plate problem was solved by the five-point scheme, but shear waves occurred (Fig. 4-8). These could neither be controlled by the angle q nor by the Navier-Stokes q. Several corrective schemes were tried. The stabilizing effect was good for considerable length of time but eventually instability occurred.

For rotationally symmetric problems the five-point scheme is considerably more stable. Figures 4-9 and 4-10 show a circular plate with a hole clamped at the outer edge. It is significant that the corners on the inner edge remain stable. Eventually the integration becomes unstable, however, although the grid remains smooth.

Results obtained with the four-node element scheme have shown good comparison with those reported by Wilkins as far as amplitude and frequency of the vibrating plate is concerned (Fig. 4-11). Unfortunately an hourglass distortion appears. This should be controllable by a higher coefficient for the angle damping coefficient.

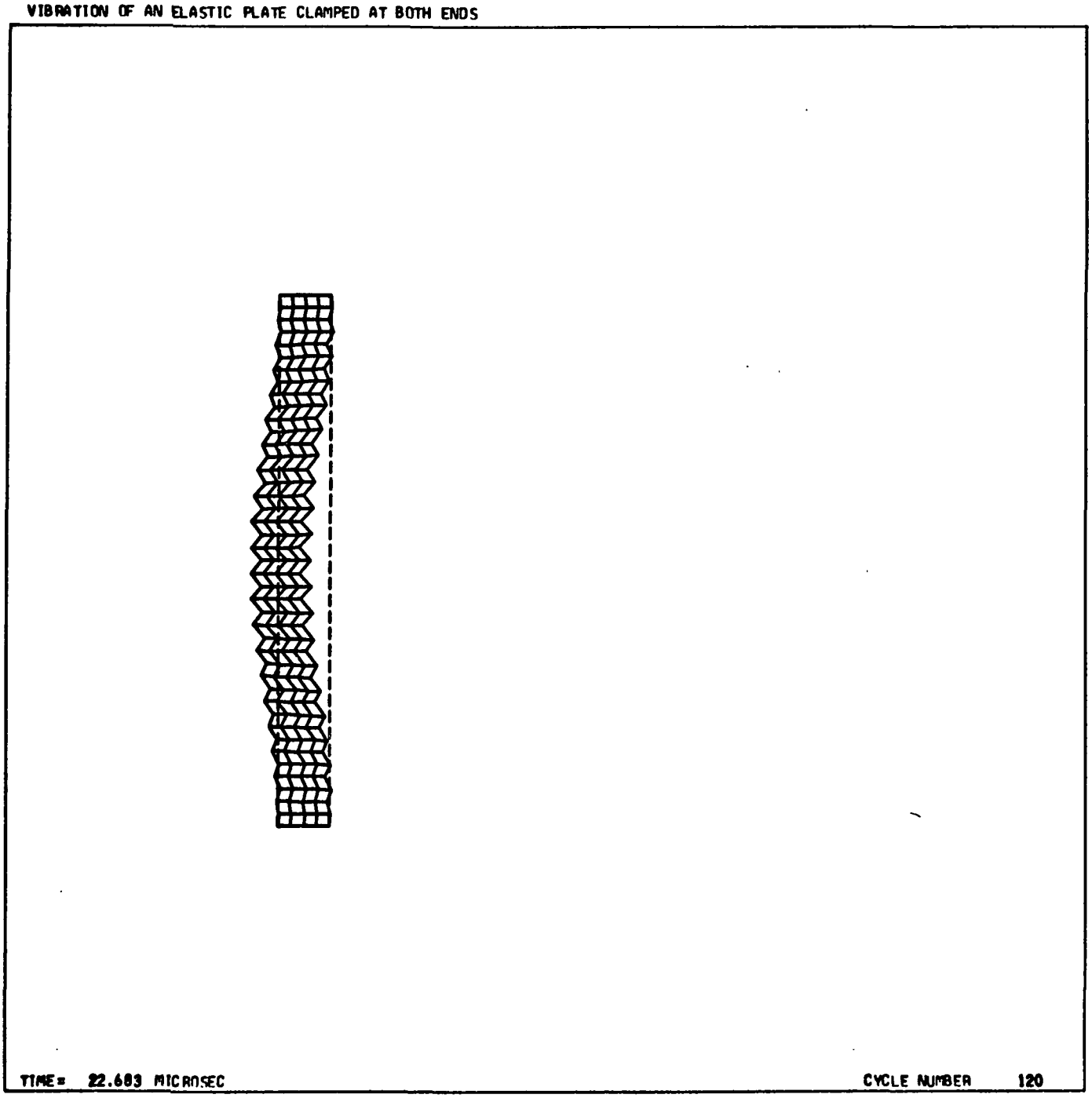

Fig. 4-8 - Shear Waves in Elastic Plate (Five-Point Scheme, Plane Strain)

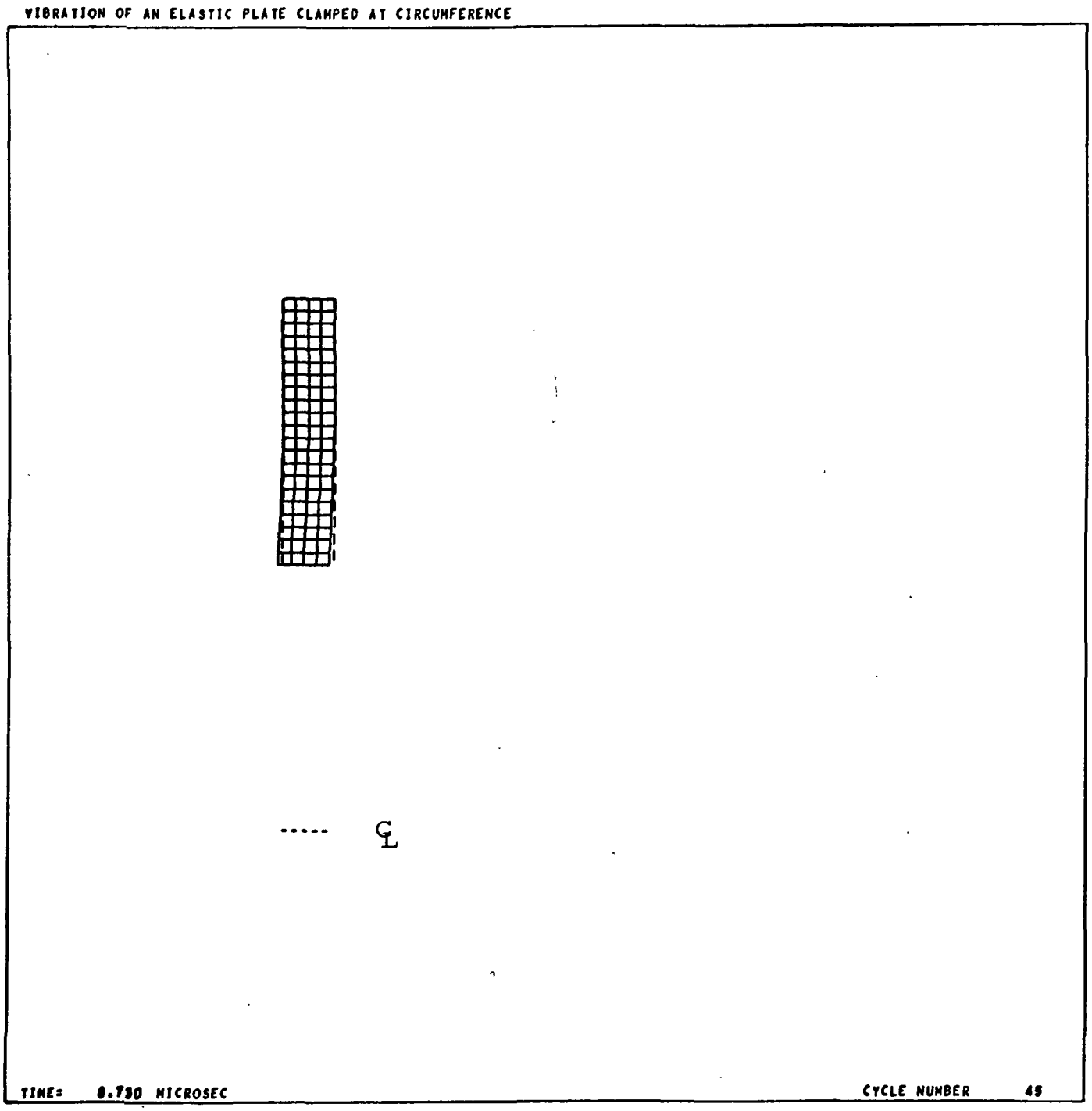

Fig. 9 - Cutoff at t = 8μ sec

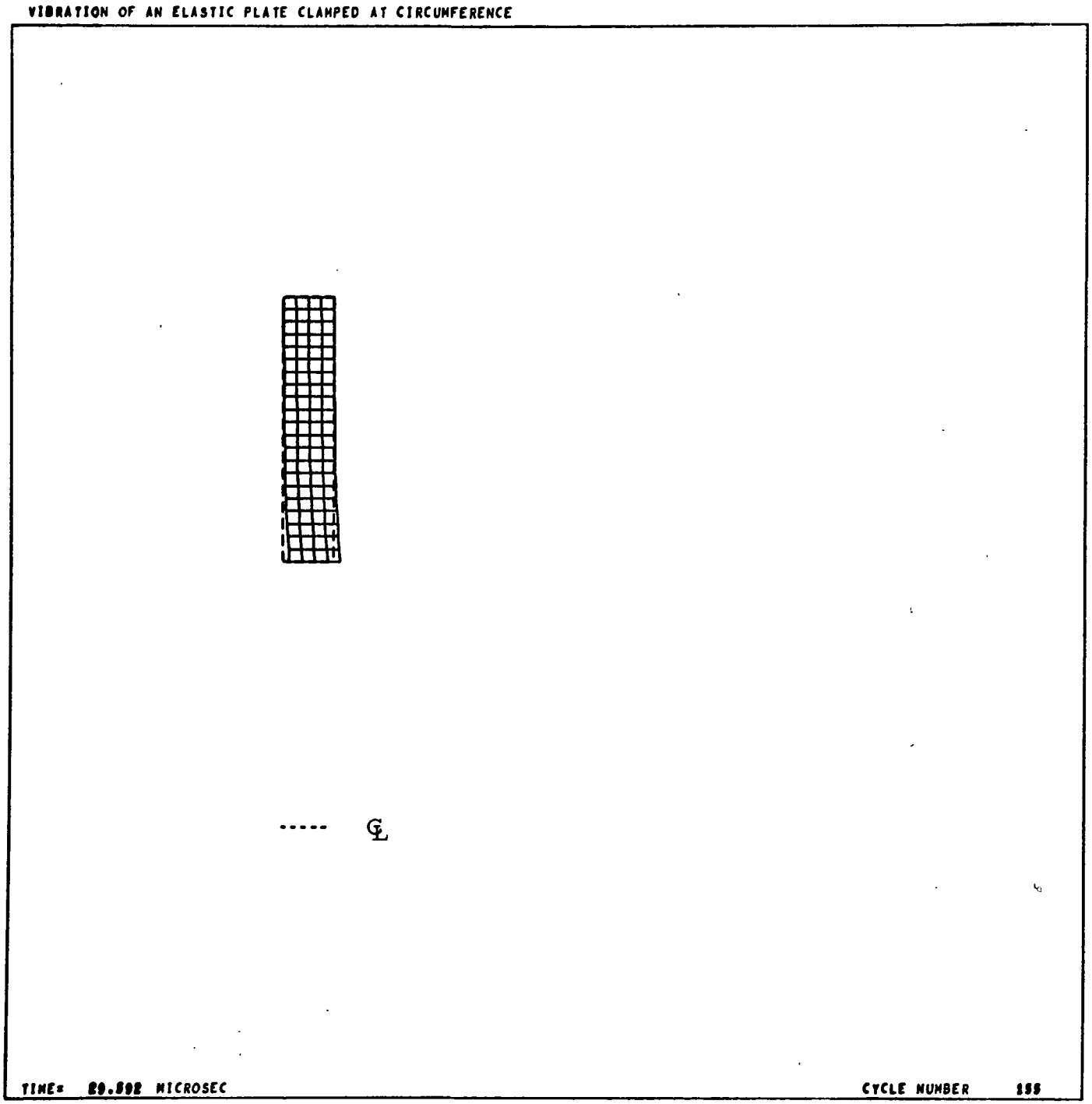

Fig. 4-10 - The Grid Moves to the Other Side

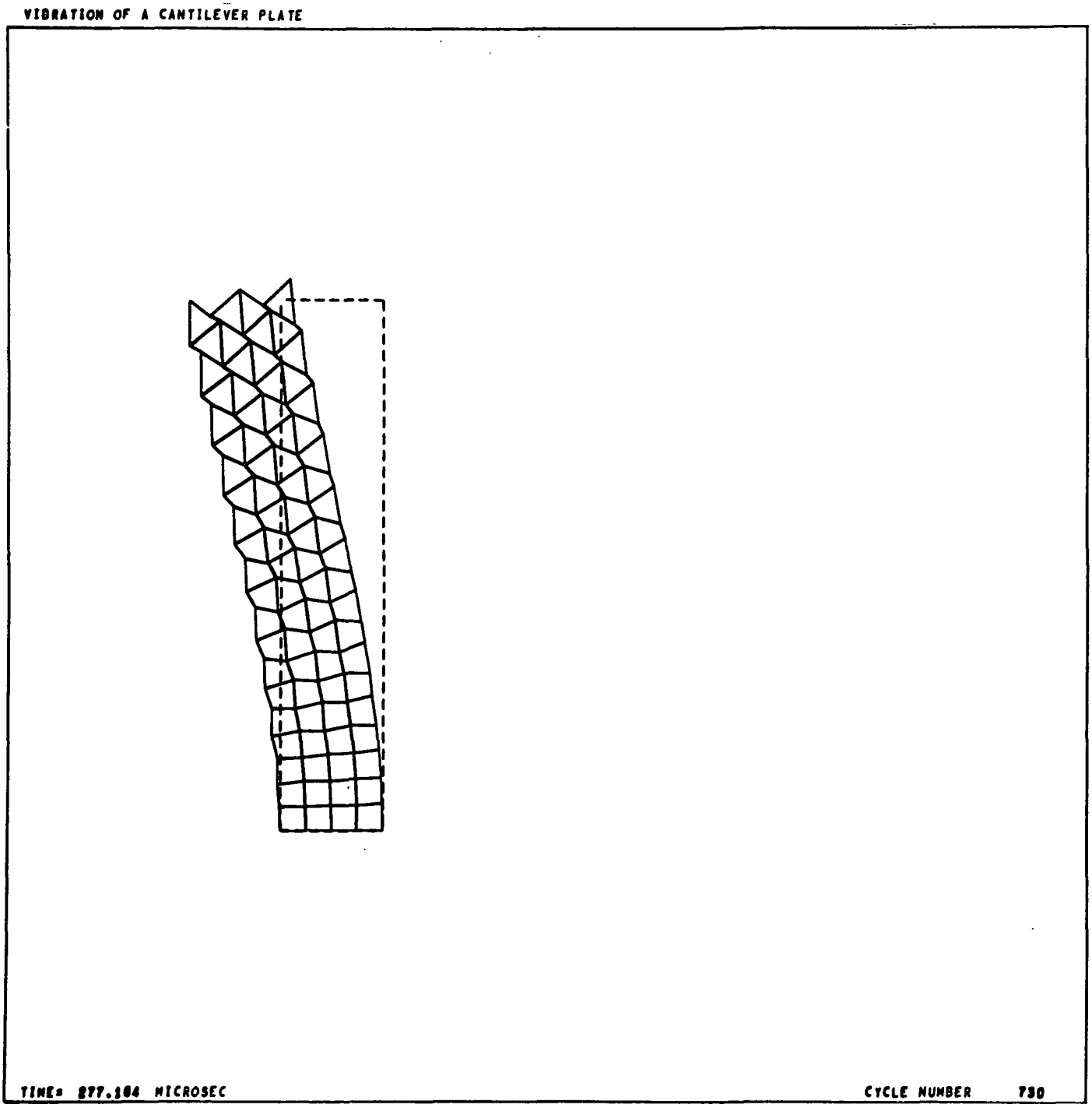

Fig. 4-11 - Bending of a Cantilever Plate Showing Hourglass Distortion

Section 5
CONCLUSIONS AND RECOMMENDATIONS

In order to analyze the behavior of a spacecraft structure subjected to a meteorite impact two numerical analogs to the governing differential equations related to elastic-plastic flow and fracture of a material have been developed and computer programs have been written to perform the calculations. Of these two schemes, the finite element or four-node scheme appears to be superior for the following reasons.

- Stability problems appear to be only of the "hourglass" type and may be controlled.
- It is simpler to formulate
- The boundary condition treatment is simple to apply.

Full production versions have not been created with either method. Stability problems occupied more effort than originally anticipated and thus detracted from development of a user-oriented analysis.

It can be said, however, at least regarding the finite element scheme that the major problems have been overcome and that a nominal amount of future development will, in fact, produce a utilitarian program.

During the course of the study the fracture condition itself was not thoroughly investigated, but no undue problems are anticipated.

It is concluded that further exercise of the existing programs and further development is warranted.

Section 6
REFERENCES

1. MacCormack, R. W., "The Effect of Viscosity in Hypervelocity Impact Cratering," AIAA paper C9-364 (1969).

2. Rosenblatt, M., "Analytical Study of Strain Rate Effects in Hypervelocity Impacts," NASA-CR-61323, January 1970.

3. Read, H. E., and R. C. Bjork, "A Numerical Study of the Hypervelocity Impact of a Cylindrical Projectile with a Semi-Infinite Target," Shock Hydrodynamics, Inc., August 1970.

4. Wilkins, M. L., "Calculation of Elastic-Plastic Flow," UCRL-7322, Rev. 1, Lawrence Radiation Laboratory, Livermore, Calif., 1963.

5. National Aeronautics and Space Administration, "Scientific Involvement in Skylab," by Space Sciences Laboratory of Marshall Space Flight Center; "Meteoroid Investigations by Edward Schrieber," NASA TM X-64725.

6. Ang, A. H-S., and J. H. Rainer, "Model for Wave Motions in Axisymmetric Continue," Proceedings of the American Soc. of Civil Engineers, Journal of the Engineering Mechanics Division, April 1964.

7. Ang, A. H-S., and G. N. Harper, "Analysis of Contained Plastic Flow in Plane Solids," Proceedings of the American Soc. of Civil Engineers. Journal of the Engineering Mechanics Division, October 1964.

8. Ang, A. H-S., and L. A. Lopez, "Discrete Model Analysis of Elastic-Plastic Plates," Proceedings of the American Soc. of Civil Engineers, Journal of the Engineering Mechanics Division, February 1968.

9. Hill, R., The Mathematical Theory of Plasticity, Oxford, 1950.

Appendix

USERS' MANUALS FOR THE COMPUTER PROGRAMS

A.1 FIVE-POINT SCHEME

Card	Columns	Format	Description
1	1-72	12A6	Heading
2	1-5	I5	Time step increments for output
	6-10	I5	Total number of time steps
	11-15	I5	Type of symmetry 0 = plane 1 = cylindrical
	16-20	I5	Number of stations in x-direction
	21-25	I5	Number of stations in r-direction
	26-30	I5	Type of output 0 = plots desired
3	1-10	E10.4	ρ (g/cm^3) = density
	11-20	E10.4	μ (Mb) = shear modulus
	21-30	E10.4	Y^o (Mb) = yield strength
	31-40	E10.4	F_{tu} (Mb) = ultimate tensile strength
	41-50	E10.4	C_o^2 = a constant
4	1-10	E10.4	Coefficients of equation of state a_1
	11-20	E10.4	Coefficients of equation of state a_2
	21-30	E10.4	Coefficients of equation of state a_3
5	1-10	E10.4	ℓy = length of the region in r-direction
	11-20	E10.4	ℓx = length of the region in the x-direction
	21-30	E10.4	y_a = beginning of region in r-direction (plate with hole)
	31-40	E10.4	α = magnification factor for plots
6	1-72	12A6	Message to the operator of the SC 4020 plotter.

A.2 FOUR-NODE ELEMENT SCHEME

Card	Columns	Format	Description
1	1-72	12A6	Heading
2	1-5	I5	Time step increments for output
	6-10	I5	Total number of time steps
	11-15	I5	Type of symmetry 0 = plane 1 = cylindrical
	16-20	I5	Number of stations in x-direction
	21-25	I5	Number of stations in r-direction
	26-30	I5	Type of output 0 = plots desired

Card	Columns	Format	Description
3	1-10	E10.4	ρ (g/cm^3) = density
	11-20	E10.4	μ (Mb) = shear modulus
	21-30	E10.4	F_{ty} (Mb) = yield strength
	31-40	E10.4	F_{tu} (Mb) = ultimate strength
	41-50	E10.4	C_o } = constants
	51-60	E10.4	C_s } = constants
	61-70	E10.4	C_A } = constants
	71-80	E10.4	a_s (cm/μ sec) = speed of sound
4	1-50	5E10.4	Coefficients of equation of state
5	1-10	E10.4	X_A } Boundaries of the grid
	11-20	E10.4	X_B } Boundaries of the grid
	21-30	E10.4	Y_A } Boundaries of the grid
	31-40	E10.4	Y_B } Boundaries of the grid
6	1-72	12A6	Message to the operator of the SC 4020 plotter.